Received: 30 January 2024 | Revised: 13 July 2024 | Accepted: 14 September 2024
DOI: 10.1002/mop.34335

RESEARCH ARTICLE

WILEY

A novel high-isolation dual-polarized air-patch antenna based on composite decoupling structure

Fuwang Li[1] | Yi-Feng Cheng[1,2] | Kuiwen Xu[1] | Gaofeng Wang[1]

[1]School of Electronics and Information Engineering, Hangzhou Dianzi University, Hangzhou, China

[2]Key Laboratory of Micro-nano Sensing and IoT of Wenzhou, Wenzhou Institute of Hangzhou Dianzi University, Wenzhou, China

Correspondence
Yi-Feng Cheng, School of Electronics and Information Engineering, Hangzhou Dianzi University, Hangzhou, China.
Email: chengyifeng2013@gmail.com

Funding information
Wenzhou Basic Industrial Project, Grant/Award Number: G20240045; National Natural Science Foundation of China, Grant/Award Numbers: 62141409, 62201183, 92373202; Laboratory of Flexible Electronics Technology, Tsinghua University

Abstract
This paper presents a novel wideband dual-polarized air-patch antenna with enhanced port isolation. The proposed design consists of a suspended metal patch, two feeding slots, and novel composite decoupling structures (CDS). The CDS is composed of two reactive loads (RLs), an additional square slot (ASS), and two neutralizing lines (NLs). The reactive loads and one NL are connected to the feeding slots. The other NL is connected to the ASS. The CDS plays a critical role in achieving wideband high port isolation. The decoupling principles are illustrated by using a circuit model and through rigorous mathematical derivation. Design evolution of the proposed antenna (Ant 1–5) was carefully explained. Experimental results demonstrate that the proposed antenna has a −15 dB refection coefficient bandwidth covering the frequency range of 3.32–3.67 GHz. Additionally, it exhibits high port isolation (>35 dB), low cross polarization, high gain, and excellent total efficiency (>85%).

KEYWORDS
air-patch antenna, composite decoupling structures, dual-polarized, High-isolation

1 | INTRODUCTION

Dual-polarized antennas enable in-band duplex operation, allowing simultaneous transmission and reception within the same frequency band.[1] This capability effectively reduces the antenna count and spatial requirements, offering extensive application potential and practical benefits. Port isolation plays a crucial role in assessing dual-polarized antenna performance, as it quantifies the independence between orthogonal polarizations. Various techniques[2–17] have been introduced in recent years to enhance port isolation for both single antenna (SA) and multiple antenna elements (MAE) configurations. For instance, the widely adopted approach to enhance port isolation is the utilization of a planar balun composed of a power divider and a 180-degree phase shifter.[2–4] In,[5–8] the 180-degree phase difference between two ports is achieved through coupled slot lines. Alternatively, in,[9–11] the hybrid coupler (HC) is employed for differential feeding. Moreover, in,[12] the simultaneous excitation of $TM_{01\delta}$ and $HEM_{21\delta}$ modes of a Dielectric Resonator Antenna is employed to attain port decoupling without the need of additional structures. The radiating element[12–14] of dielectric resonant antenna (DRA) generally has a high profile. Furthermore, the previous design[15] involves complex 3D connecting structure between vertical feeding probes, which proved to be unstable during manufacturing. However, most aforementioned decoupling methods for dual-polarized antennas often occupy considerable space. Additionally, some methods can have adverse effects on antenna performance, such as reducing bandwidth and lowering gain and radiation efficiency.

This paper presents a novel high-isolation dual-polarized air-patch antenna featuring the composite decoupling structures. Two U-shaped feeding slots etched on the ground are employed to feed the suspended patch, resulting in wide operating bandwidth (3.32–3.67 GHz) with a return loss of −15dB. The combination of two reactive loads (RLs), an additional square slot (ASS), and two neutralizing lines (NLs) is simultaneously utilized to enhance isolation (>35 dB). Moreover, circuit model is proposed for rapid optimization. Rigorous design formulas are derived to streamline the design process. Experimental results reveal that the proposed antenna boasts a wide operating bandwidth, high port isolation, high gain and excellent radiation efficiency. Additionally, the antenna has a low profile and compact size, positioning it as a promising candidate for modern wireless communication systems.

2 | PROPOSED DESIGN

2.1 | Structure of the proposed antenna

Figure 1A,B depicts the geometric structure of the proposed dual-polarized patch antenna. It consists of a suspended square metal patch fed by two U-shaped slots etched on the ground plane. The suspended patch is fabricated using 1 mm thick copper material. The microstrip structures, including feeding lines, RLs, and NLs, are printed on the bottom side of a substrate made from Rogers4003 material with a permittivity of 3.55 and a loss tangent of 0.0027. Detailed dimensions of the antenna and decoupling structures are provided in Figure 1C.

As illustrated in Figure 1A, the CDS of the proposed antenna comprises two reactive loads (RLs), an additional square slot (ASS), and two neutralizing lines (NLs). The RLs are located at the outer corners of the U-shaped slots, with their terminals connected to the ground via cylindrical holes. The one NL is connected at the inner corners of the slots. The RLs and one NL (RLANL) serves to enhance isolation between ports and achieve broadband decoupling. The ASS and the other NL (ASSANL) is designed to create a deep transmission zero (TZ). Impedance matching is achieved through adjustments to the patch width, feeding slot length, and feeding line position. Figure 1A,B displays the layout structure of the proposed dual-polarized patch antenna Table 1.

TABLE 1 Dimensions of the proposed high-isolation dual-polarized patch antenna (units: mm).

wg	wp	wf	ws	wl
50	1.2	1.85	1.0	2.0
dl	lf	wt	lt	wd
6.2	1.85	1.0	14.4	1.2
wn	nu	w	hp	
1.6	6.0	28	6.0	

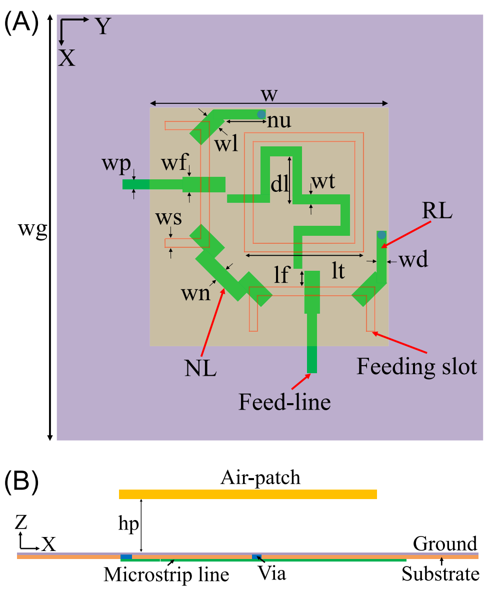

FIGURE 1 The proposed antenna. (A) Top view. (B) Side view.

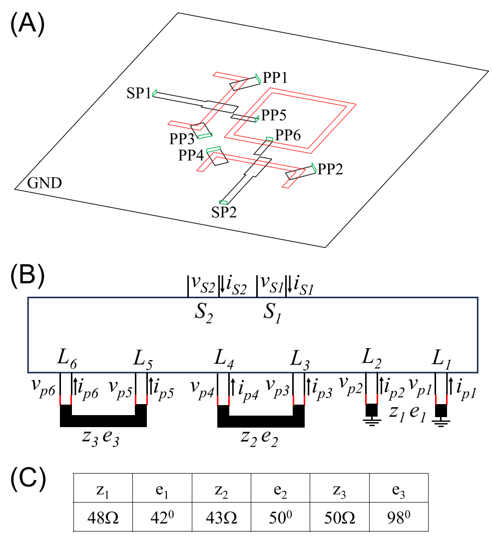

FIGURE 2 Circuit model. (A) Illustration of parasitic ports. (B) Circuit model with RLs and NLs. (C) The optimized circuit parameters of the RLs and NLs.

2.2 | Circuit model

To provide a clearer explanation, the portion of the RLs and two NLs is initially removed and replaced with parasitic ports (PPs). As depicted in Figure 2A, the proposed antenna is represented as an eight-port network (composed of two feeding ports and six PPs). The CDS employs the decoupling principle of replacing the microstrip line structure in RL and two NLs with PPs. The optimal configuration of the microstrip lines, including their electrical length and characteristic impedance, can be efficiently determined through circuit optimization. This approach significantly reduces both time and EM computational resources.

The circuit model schematic of the proposed antenna, incorporating the RLs and NLs are presented in Figure 2B. For the CDS, the short-circuited transmission lines (z_1, e_1) can be treated as the RLs. The NLs are represented by transmission lines (z_2, e_2) and (z_3, e_3). Using the method described in,[16] the two-port Y matrix of the antenna after adding RLs and TLs can be calculated as follows.

$$Y^A = Y_{11} + Y_{12}(Y_L - Y_{22})^{-1}Y_{21} \tag{1}$$

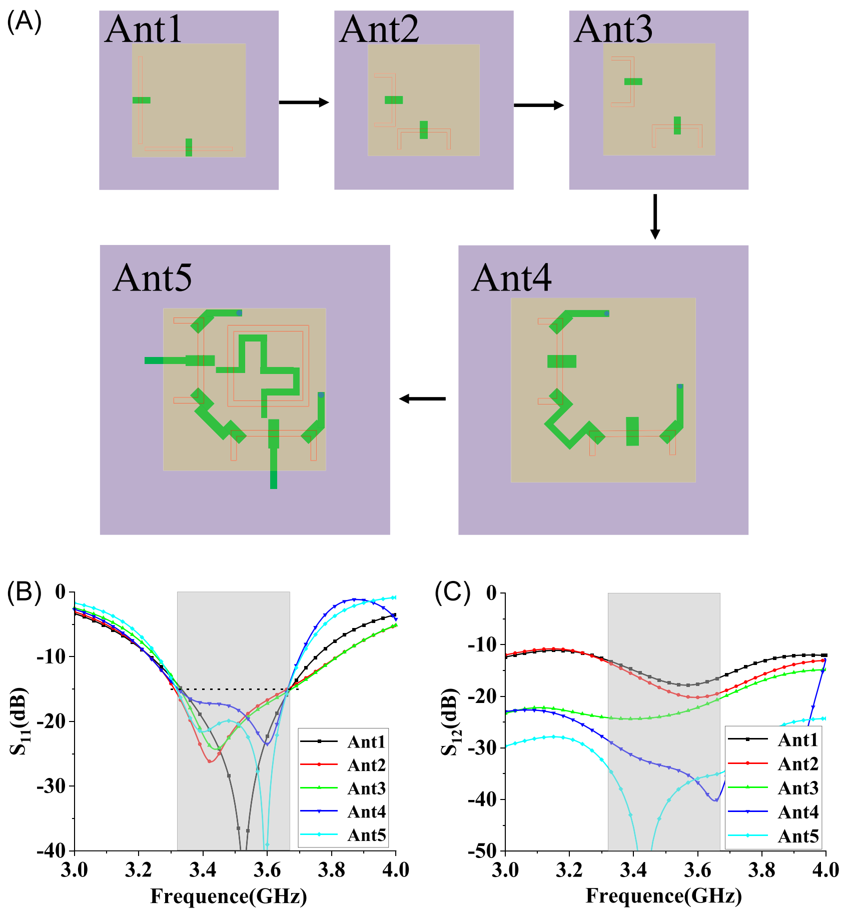

FIGURE 3 Evolution of the proposed antenna (Ant 1–5). (A) Structure. (B) S_{11}. (C) S_{21}.

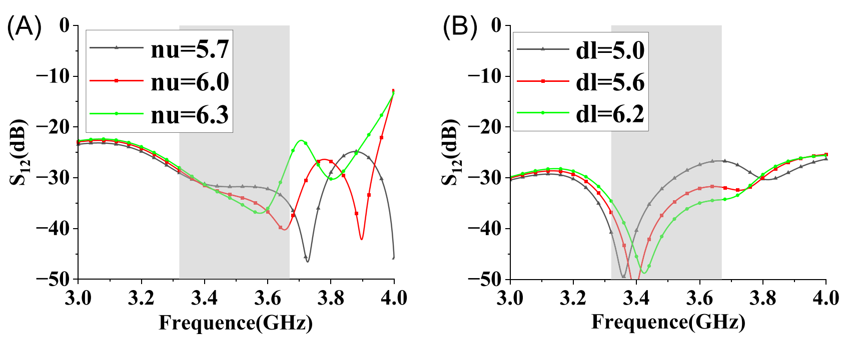

FIGURE 4 Key parameters study. (A) With RLANL (Ant 4). (B) With RLANL and ASSANL (Ant 5).

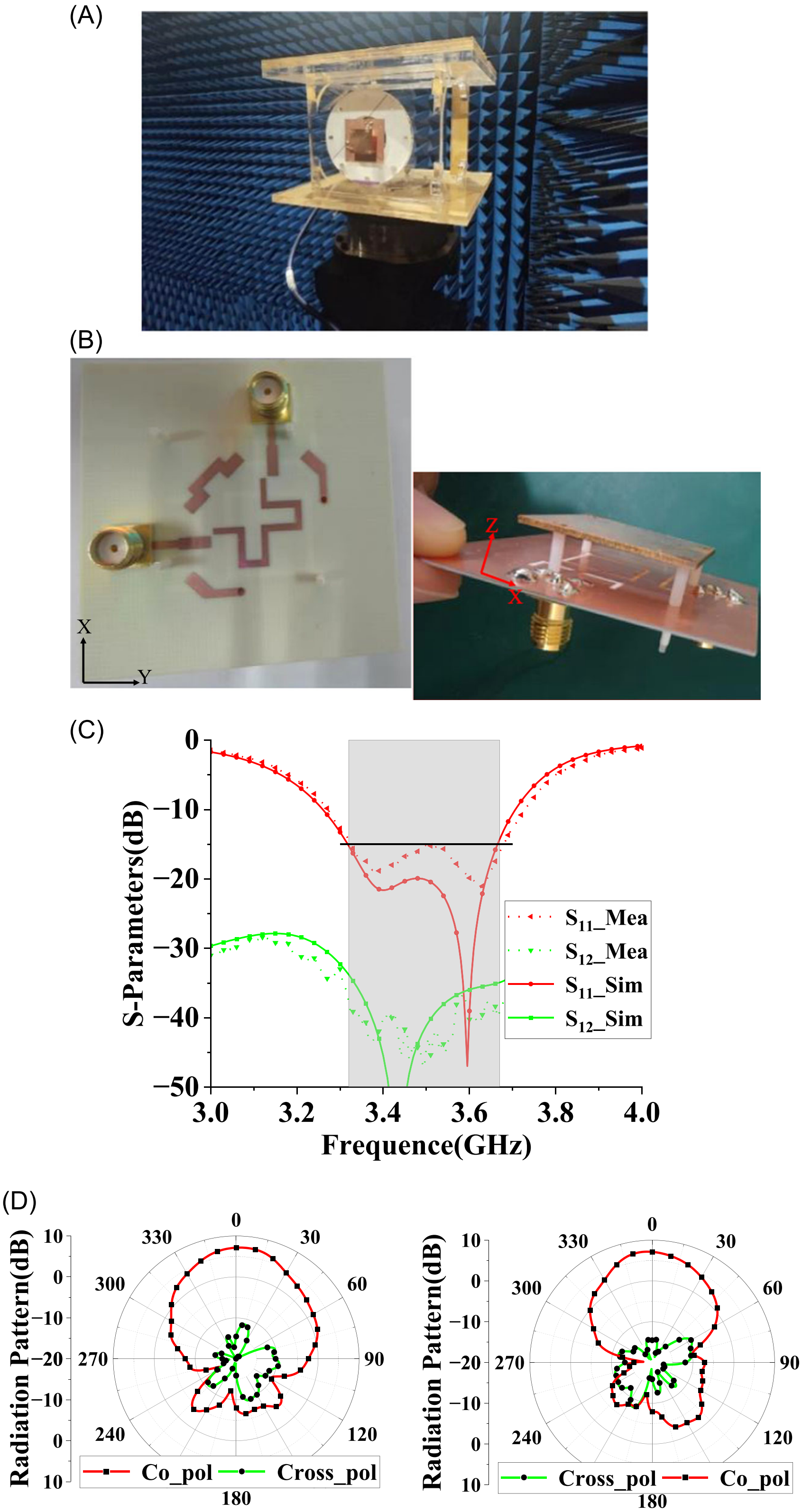

FIGURE 5 The proposed antenna. (A) Photograph of fabricated antenna inside the anechoic chamber. (B) Photographs of fabricated antenna. (C) Simulated and measured S-parameters. (D) Measured radiation patterns (*yoz*-plane and *xoz*-plane).

Where Y^A is the realized admittance matrix (after adding RLs and NLs). While Y_{11} is the self-admittance matrix (before adding RLs and NLs) of two feeding ports. Y_{21} and Y_{12} are the mutual-admittance matrixes between feeding ports and parasitic ports. And Y_{22} is the admittance matrix of parasitic ports. Y_L is the admittance matrix of the RLs and NLs, which can be further expressed as follows.

$$YL = \begin{bmatrix} R & 0 \\ 0 & K \end{bmatrix} \tag{2}$$

$$R = \begin{bmatrix} j\cot e_1/z_1 & 0 \\ 0 & j\cot e_1/z_1 \end{bmatrix} \tag{3}$$

for i = 2, 3,

$$K = \begin{bmatrix} M_2 & 0 \\ 0 & M_3 \end{bmatrix} \tag{4}$$

$$M_i = \begin{bmatrix} j\cot e_i/z_i & -j/z_i \sin e_i \\ -j/z_i \sin e_i & j\cot e_i/z_i \end{bmatrix} \tag{5}$$

As shown in Equation (1), the realized admittance matrix Y^A is a function of circuit parameters z_1, e_1, z_2, e_2, and z_3, e_3. Next step is to minimize the mutual admittance $Y^A{}_{21}$ by adjusting the corresponding circuit parameters. The optimized parameters are listed in the following Figure 2C. After abstain the optimal values, the EM structure can be then constructed to build the complete antenna system.

2.3 | Structure evolution of the proposed antenna

To elucidate the antenna's operation, Figure 3 presents the evolutionary process and its corresponding performance. Initially (Ant. 1), the feed lines and slots are positioned at the center of the patch. At this stage, the microstrip feed lines is very short and is only used to transmit signals, and the slots have an I-shaped configuration. Subsequently (Ant. 2), the feed lines remain centered on the patch, but the coupling slots take on a U-shaped design. In the third iteration (Ant. 3), the feed lines and slots are offset by 6 mm from the center position, while the slots retain their U-shaped configuration. Antennas 4 and 5 (the proposed design) are developed based on the configuration of RLANL and ASSANL. It is worth noting that the structure of antennas 1–5 evolved step by step.

In Figure 3B, the reflection coefficients of the five steps (antenna 1–5) exhibit a consistent −15 dB impedance bandwidth. As depicted in Figure 3C, the antenna decoupling performance demonstrates gradual improvement from Antenna 1 to 5. The isolation of antenna 1, being the most original dual polarization antenna with slot feed, is the lowest among all. By simply altering the slot's shape and position, the isolation of antenna 2 and 3 increased moderately. Antennas 4 and 5 were proposed to maximize isolation with RLANL and ASSANL. The worst isolation (antenna 1–5) within the specific frequency bands (3.32–3.67 GHz) is as follows: 12 dB, 13 dB, 19.5 dB, 27.5 dB, and 35 dB, respectively. The decoupling enhancements observed in antenna 1–5 can be attributed to an increasing isolation on both the lower and upper frequency bands, ultimately resulting in an isolation exceeding 35 dB (antenna 5) across the entire −15dB operating frequency band. It is worth noting that all the decoupling structures employed to improve isolation between the two ports are situated beneath the patch and do not extend beyond it, contributing to a compact overall antenna size.

For a more in-depth analysis, Figure 4 presents the comparison of key parameters of the proposed patch antenna with RLANL (Ant4) and the one with both RLANL and ASSANL (Ant5). Notably, the length of RLs in RLANL (nu) and the length of NL in ASSANL (dl) are identified as crucial factors. Exceptional decoupling performance, evaluated across the entire −15dB operating band (3.32–3.67 GHz), is achieved when nu = 6.0 mm and dl = 5.6 mm. As depicted in Figure 4A and b, varying nu and dl results in a shift of the decoupling zero, with nu affecting the upper band when RLANL is used and dl influencing the lower band when both RLANL and

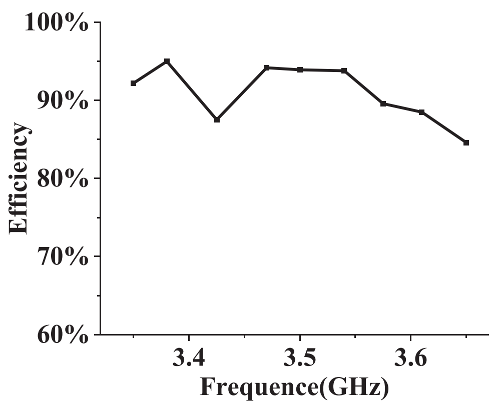

FIGURE 6 Measured total efficiency of the proposed antenna.

TABLE 2 Comparison with the previous dual-polarized antennas.

[Ref. No], year	Feed Method	Frequency (GHz)	Isolation (dB)	Decoupled Method	Total Efficiency	Dimension (λ_{min}^3)
[1] 2023	Single feed	3.3–3.8 (RL > 12 dB)	>21	metal rods	90	0.82×0.82×0.10
[2] 2023	Differential feed	5.02–5.96 (RL > 10 dB)	>42	wideband balun	N.A	2.0×2.0×0.49
[7] 2023	Differential feed	4.81–5.72 (RL > 10 dB)	>45	Marchand balun	92	0.96×0.88×0.05
[13] 2019	Differential feed	3.3–4.2 (RL > 15 dB)	>30	ME dipole	89	0.66×0.66×0.09
This work	**Single feed**	**3.32–3.67 (RL > 15 dB)**	**>35**	**CDS**	**95**	**0.55×0.55×0.07**

ASSANL are employed. Additionally, these adjustments have an impact on the decoupling performance, with decoupling becoming worse or better as nu and dl increase, respectively.

3 | EXPERIMENTAL VERIFICATION

To validate the proposed design, the dual-polarized patch antenna was designed, fabricated, and measured. Figure 5A displays images of the fabricated antennas, where the suspended patch is supported by four plastic posts. S-parameter measurements were conducted using the Keysight vector network analyzer E5071C, and radiation patterns were captured in an anechoic chamber. As depicted in Figure 5B, the measured reflection coefficient of the proposed antenna remains below −15 dB within the frequency range of 3.32–3.67 GHz. The simulation and measured results exhibit consistency, with a reasonable level of error between them. This can be attributed to various factors such as machining errors, plate errors, excitation SMA head errors, nylon plastic post errors, and environmental effects that occur during the actual processing and testing. The introduced decoupling approach, involving slot modifications and the incorporation of RLANL and ASSANL, achieves high isolation (>35 dB) throughout the entire −15 dB operating band. Figure 5C shows the measured radiation patterns in the *yoz*- and *xoz*-planes of the proposed antenna. Furthermore, Figure 5D provides measured results of the radiation efficiency for the proposed antenna, revealing high total efficiency (95%) and impressive antenna gain (7.5 dBi) Figure 6.

Table 2 presents a performance comparison between the proposed antenna and other recent published dual-polarized antennas. As demonstrated, this design performs competitively compared to existing proposals, particularly in terms of isolation, efficiency, and compact dimension. For example, the size of this proposed antenna is only $0.55\lambda_{min} \times 0.55\lambda_{min} \times 0.07\lambda_{min}$ (λ_{min} is the wavelength corresponding to the lowest operating frequency) and the efficiency is 95%. The proposed antenna is a promising candidate for current and future wireless communication systems.

4 | CONCLUSION

In this paper, a novel dual-polarized air-patch antenna with enhanced isolation based on CDS is proposed, designed, and demonstrated. This antenna shows remarkable characteristics, including high isolation and a wide operating bandwidth of. To elucidate the decoupling principle more effectively, the antenna's circuit model is analyzed, incorporating RLs and the NLs, utilizing the PP method. Additionally, throughout the design evolution of Ant 1–5, the isolation between the two ports consistently increases. Ultimately, a high isolation level (improved by 23 dB) between the two input ports is achieved.

ACKNOWLEDGMENTS

The authors would like to thank Faraday Dynamics, Ltd.[18] for providing useful simulation software (SuperEM) to assist the research in this paper. This work was supported in part by the National Natural Science Foundation of China under Grant 62201183, 92373202 and 62141409, and in part by the Fundamental Research Projects of Wenzhou Municipality under Grant G20240045.

DATA AVAILABILITY STATEMENT

Data sharing is not applicable to this article as no new data were created or analyzed in this study.

ORCID

Yi-Feng Cheng http://orcid.org/0000-0002-2364-0372
Kuiwen Xu http://orcid.org/0000-0002-4943-5668
Gaofeng Wang http://orcid.org/0000-0001-8599-7249

REFERENCES

1. Yoon T, Oh J. Metal rods-based field concentrated common and differential modes theory enabling design of dual-polarized antennas. *IEEE Trans Antennas Propag*. 2023;11(4):427-430.
2. Le-Huu T, Ta SX, Nguyen KK, Dao-Ngoc C, Nguyen-Trong N. Differential-fed dual-polarized filtering Fabry-Perot antenna with high isolation. *IEEE Access*. 2022;10:94616-94623.
3. Ta SX, Nguyen-Trong N, Nguyen VC, Nguyen KK, Dao-Ngoc C. Broadband dual-polarized antenna using metasurface for full-duplex applications. *IEEE Antennas Wireless Propag Letter*. 2021;20(2):254-258.
4. Feng B, He X, Cheng J-C, Zeng Q, Sim C-Y-D. A low-profile differentially fed dual-polarized antenna with high gain and isolation for 5G microcell communications. *IEEE Trans Antennas Propag*. 2020;68(1):90-99.
5. Ta SX, Nguyen-Trong N. Analysis and design of an ultra-wideband Dual-polarized antenna for IBFD applications. *IEEE Trans Antennas Propag*. 2022;70(11):11121-11126.
6. Kuznetcov MV, Podilchak SK, McDermott AJ, Sellathurai M. Dual-polarized antenna with dual-differential integrated feeding for wideband full-duplex systems. *IEEE Trans Antennas Propag*. 2021;69(11):7192-7201.
7. Zhang X-K, Ke Y-H, Wang X-Y, Tang S-C, Chen J-X. Broadband dual-polarized dielectric patch antenna with high isolation for full-duplex communication. *IEEE Antennas Wireless Propag Letter*. 2023;22(4):878-882.
8. Tang H, Tong C, Chen JX. Differential dual-polarized filtering dielectric resonator antenna. *IEEE Trans Antennas Propag*. 2018;66(8):4298-4302.
9. Wojcik D, Surma M, Noga A, Magnuski M. High port-to-port isolation dual-polarized antenna array dedicated for full-duplex

base stations. *IEEE Antennas Wireless Propag Letter*. 2020;19(7):1098-1102.
10. Bui TH, Vu HT, Ta SX, Nguyen KK, Dao-Ngoc C, Nguyen-Trong N. Dual-band dual-polarized slotted-patch antenna for in-band full-duplex applications. *IEEE Antennas Wireless Propag Letter*. 2023;22(6):1286-1290.
11. Nawaz H, Tekin I. Dual-polarized, differential fed microstrip patch antennas with very high interport isolation for full-duplex communication. *IEEE Trans Antennas Propag*. 2017;65(12):7355-7360.
12. Ma CJ, Zheng SY, Pan YM. Millimeter-wave co-polarized in-band full-duplex antenna based on a mode superposition method. *IEEE Trans Antennas Propag*. 2023;71(6):4675-4685.
13. Liu N-W, Liang Y-D, Zhu L, Fu G, Liu Y, Yun Y. Electric-field null bending of a single dual-port patch antenna for co-linear polarization decoupling using characteristic modes analysis. *IEEE Trans Antennas Propag*. 2022;70(12):12247-12252.
14. Pan YM, Hu Y, Zheng SY. Design of low mutual coupling dielectric resonator antennas without using extra decoupling element. *IEEE Trans Antennas Propag*. 2021;69(11):7377-7385.
15. Li F, Cheng Y-F, Wang G, Luo J. A novel high-isolation dual-polarized patch antenna with two in-band transmission zeros. *Micromachines*. 2023;14(9):1784.
16. Cheng Y-F, Cheng K-KM. Decoupling of 2 × 2 MIMO antenna by using mixed radiation modes and novel patch element design. *IEEE Trans Antennas Propag*. 2021;69(12):8204-8213.
17. Yang SJ, Pan YM, Zhang Y, Gao Y, Zhang XY. Low-profile dual-polarized filtering magneto-electric dipole antenna for 5G applications. *IEEE Trans Antennas Propag*. 2019;67(10):6235-6243.
18. V.2023 SuperEM. Faraday Dynamics, Inc., Hangzhou, Zhejiang, China, 2023.

How to cite this article: Li F, Cheng Y-F, Xu K, Wang G. A novel high-isolation dual-polarized air-patch antenna based on composite decoupling structure. *Microw Opt Technol Lett*. 2024;66:e34335. doi:10.1002/mop.34335